LOW-REYNOLDS NUMBER EFFECTS IN VENTILATED ROOMS: A NUMERICAL STUDY

L. Davidson,[*] P.V. Nielsen and C. Topp

Dept. of Building Technology and Structural Engineering
Aalborg University, Denmark

ABSTRACT

In ventilated rooms the flow is often not fully turbulent because the Reynolds number is too low. When the flow is not fully turbulent, the traditional RANS (Reynolds Averaged Navier-Stokes) method employing $k - \varepsilon$ or $k - \omega$ is not suitable, because this method has difficulties in treating regions where the flow is laminar or not fully turbulent. There exist a number of low-Re number $k - \varepsilon$ and $k - \omega$ models, but they have all been designed to treat low-Re number effects close to walls, not regions where the flow becomes laminar far from the walls, as occurs in ventilated rooms. In the present study, we use Large Eddy Simulations (LES) which is a suitable method for simulating the flow in ventilated rooms at low Reynolds number.

EQUATIONS

With a spatial, inhomogeneous filter (denoted by a bar) applied to the incompressible Navier-Stokes equations, we obtain the momentum and continuity equations for the large scale motion

$$\frac{\partial \bar{u}_i}{\partial t} + \frac{\partial}{\partial x_j}\left(\bar{u}_i \bar{u}_j\right) = -\frac{1}{\rho}\frac{\partial \bar{p}}{\partial x_i} + \nu \frac{\partial^2 \bar{u}_i}{\partial x_j \partial x_j} - \frac{\partial \tau_{ij}}{\partial x_j}, \quad \frac{\partial \bar{u}_i}{\partial x_i} = 0 \tag{1}$$

where the subgrid stress tensor is given by $\tau_{ij} = \overline{u_i u_j} - \bar{u}_i \bar{u}_j$, and is modelled as

$$\tau_{ij} = -2\nu_{sgs}\bar{S}_{ij} = -2C_{hom}^k \Delta k_{sgs}^{\frac{1}{2}}\bar{S}_{ij}, \quad \bar{S}_{ij} = \frac{1}{2}\left(\frac{\partial \bar{u}_i}{\partial x_j} + \frac{\partial \bar{u}_j}{\partial x_i}\right). \tag{2}$$

[*]on leave from Dept. of Thermo and Fluid Dynamics, Chalmers University of Technology

The Dynamic One-Equation Model

In the present study, a one-equation dynamic subgrid model (Davidson 1997) is used. In this model, the modeled k_{sgs} equation can be written

$$\frac{\partial k_{sgs}}{\partial t} + \frac{\partial}{\partial x_j}(\bar{u}_j k_{sgs}) = \frac{\partial}{\partial x_j}\left(C^k_{hom}\Delta\, k_{sgs}^{\frac{1}{2}}\frac{\partial k_{sgs}}{\partial x_j}\right) + P_{k_{sgs}} - C^k_* \frac{k_{sgs}^{\frac{3}{2}}}{\Delta} \tag{3}$$

In the production term, the dynamic coefficient C^k is computed in a way similar to that used in the standard dynamic model (Davidson 1997). The coefficient in front of the dissipation term C^k_* is computed by assuming that the transport of the SGS kinetic energy on the grid level (k_{sgs}) is equal to the transport of the SGS kinetic energy on the test level (K). The production term in the k_{sgs} equation is computed as

$$P_{k_{sgs}} = -2C^k\Delta k_{sgs}^{\frac{1}{2}}\bar{S}_{ij}\bar{S}_{ij} \tag{4}$$

Please note that in the production term a *local* coefficient C^k is used, whereas in the momentum equations and in the diffusion term in the k_{sgs} equation a homogeneous (constant) coefficient C^k_{hom} is used. For more details, see Davidson (1997), Krajnović and Davidson (1999) and Sohankar, Davidson, and Norberg (2000).
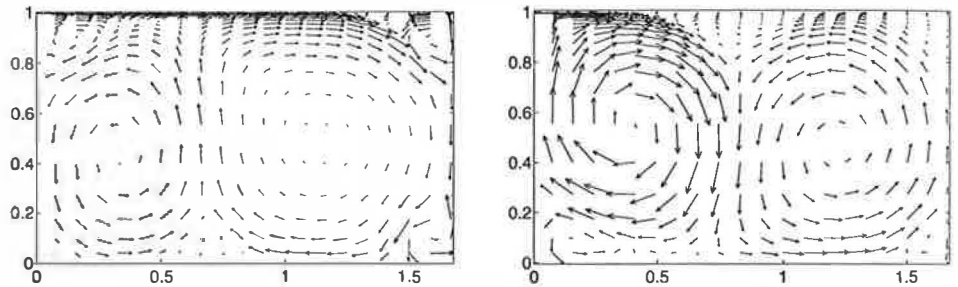

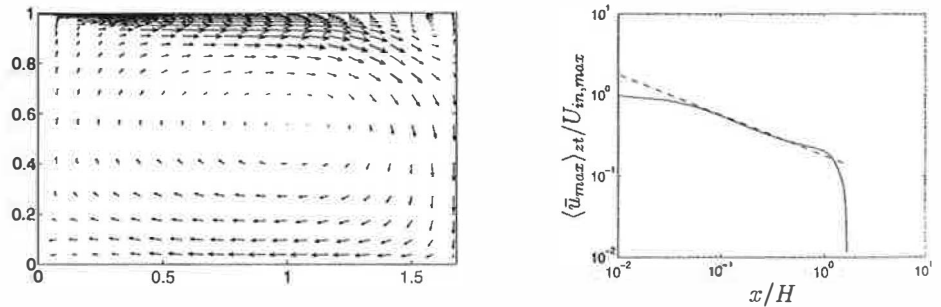FIGURE 1: Unsteady, 2D laminar computations. Time-averaged flow field. Left: QUICK; right: central differencing.

FIGURE 2: LES. Left: predicted velocity field $\langle\bar{u}\rangle_{zt}$ and $\langle\bar{v}\rangle_{zt}$. Right: peak velocity along the ceiling (solid line); the dashed line represents $\bar{u}/U_{in,max} = K_p(x/h)^{-1/2}$ with $K_p = 2.03$.

RESULTS

A finite volume code is used. For space discretization, central differencing is used for all terms. (For the 2D, unsteady, laminar computation, either the QUICK scheme or the central-differencing scheme was used for the convective terms.) Crank-Nicolson scheme is used for time discretization.

The inlet is located at the left wall, immediately below the ceiling. The outlet is located at the left wall immediately above the floor. The Reynolds number is $Re = U_{in}h/\nu = 600$ (where U_{in} denotes the bulk velocity) and $L/H = 1.68$, $W/H = 1.44$, $h/H = 0.008$. Inlet and outlet extend over the whole width of the room.

The boundary conditions are as follows. At the inlet we have laminar flow, i.e. $\bar{v} = \bar{w} = k_{sgs} = 0$ and a parabolic profile for $\bar{u}$. At all walls $\bar{u} = \bar{v} = \bar{w} = k_{sgs} = 0$. At the outlet a constant $\bar{u}$ is set from global continuity. The streamwise gradient is set to zero for the other variables. The normal gradient of $\bar{p}$ is set to zero at all boundaries.

A $80 \times 80 \times 48$ mesh is used. Constant spacing is used in the x and z directions. The cell near the floor ($y = 0$) has $\Delta y/H = 0.0105$. The cells are then stretched by 8% in the y direction up to $y/H = 0.5$ (cell 1 to 22). From $y/H = 0.5$ the cells are compressed by 8% up to $y/H = 0.992$. Ten cells (constant Δy) cover the inlet.
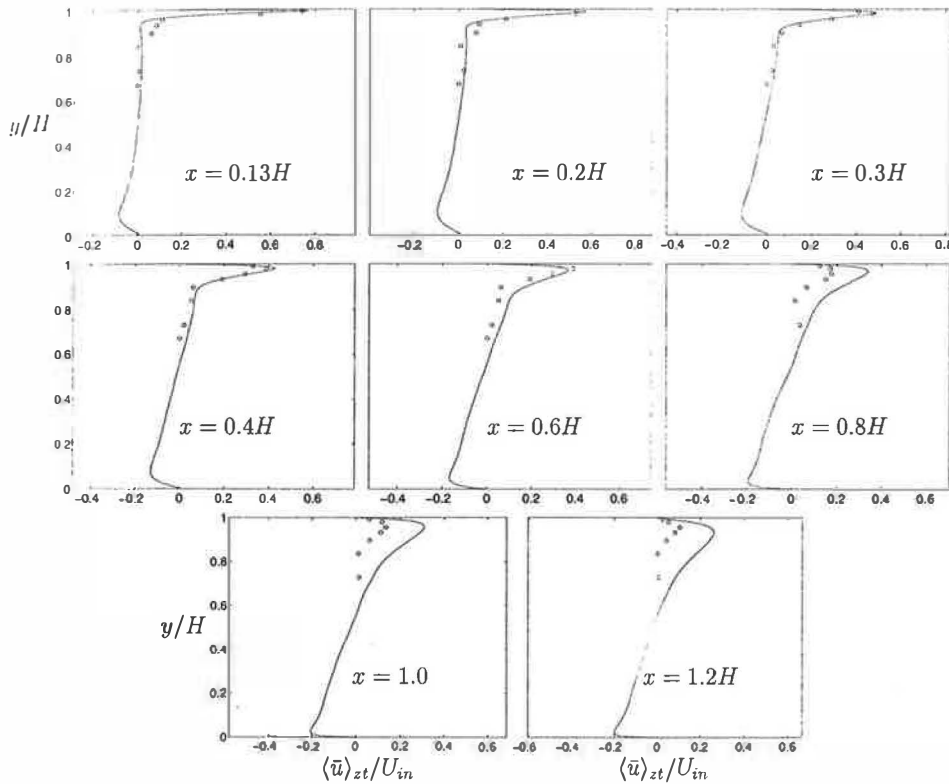

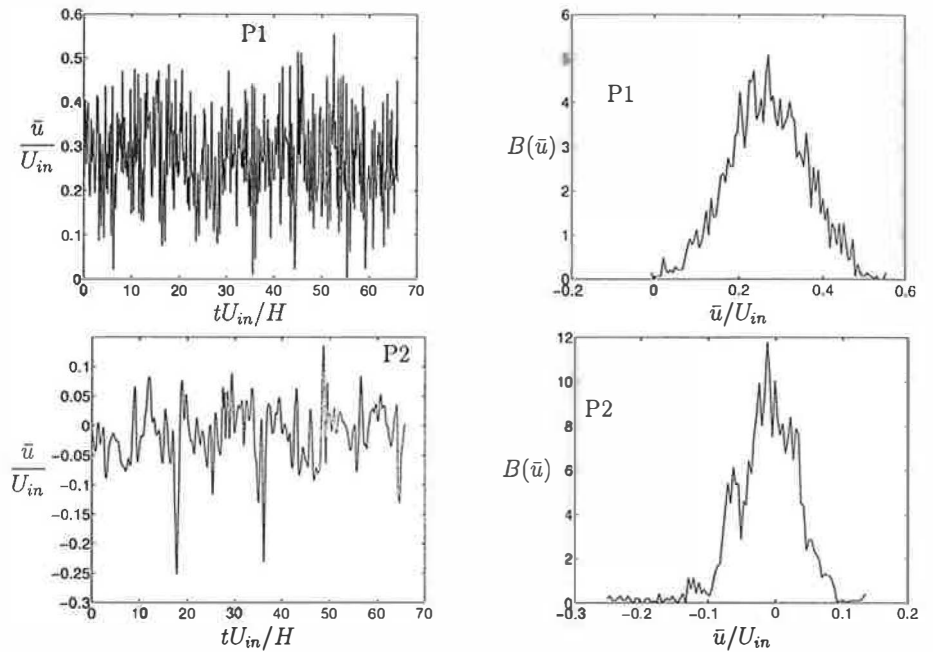FIGURE 3: Velocity profiles. Lines: LES; markers: experiments.

FIGURE 4: Left: time history. Right: probability function. Point P1: $x = 0.3H$, $y = 0.997H$, $z = 0.5W$; point P2: $x = 1.3H$, $y = 0.997H$, $z = 0.5W$.

Unsteady Laminar Two-Dimensional Flow

Initially we assumed that flow was fully laminar, and we computed the flow by solving the unsteady, laminar, two-dimensional equations. We used two different discretization schemes for the convective terms: the QUICK scheme and the central-differencing scheme. The time-averaged flow fields are presented in Fig. 1. When the QUICK scheme is used the wall jet stays attached to the ceiling up to $x \simeq 1.2H$. When, however, the central-differencing scheme is used, the wall jet detaches from the ceiling at $x \simeq 0.5H$ and falls down to the floor. The reason is believed to be due to the fact that the QUICK scheme is dissipative but the central-differencing scheme is not. That a scheme is dissipative means that it dampens oscillations, both numerical as well as physical ones. The central-differencing scheme does thus not dampen the oscillations in the wall jet, oscillations which may both be numerical as well as physical due to unsteadiness. The oscillations increase the entrainment into the wall jet. This is probably the main reason why the predicted wall jet falls down to the floor when central differences are used.

RANS With $k - \omega$ Model

Some attempts to compute the flow using a traditional RANS have also been carried out. The CALC-BFC code was used together with the $k - \omega$ model of Peng et al. (Peng, Davidson, and Holmberg 1997). Since the inlet conditions are laminar, it is not clear which boundary conditions should be used for k and ω. The local turbulence intensity was set to 0.01, and the inlet value for ω was varied between $\omega_{in} = \sqrt{k_{in}}/(0.1h)$ (gives $\nu_{t,in} \simeq 32\nu$) with and $\omega_{in} = k/(0.1\nu)$ (gives $\nu_{t,in} = 0.1\nu$). The variations of ω_{in} did not produce any changes in the flow pattern. It should here be mentioned that $k - \omega$ models are superior in treating flow which is close to being laminar, since the ω equation behaves well even if k goes to zero. On the contrary, the ε equation in $k - \varepsilon$

models causes problems when k goes to zero, since the ε equation includes the ratio ε/k.

The predicted flow field is very different from the laminar ones. The wall jet detaches from the ceiling almost immediately after the inlet. Both the QUICK scheme and the Hybrid scheme were tested, but they gave the same predicted flow field. The predicted flow fields differ very much from the experiments, and it seems that RANS is unable to predict this kind of low-Re number flow.

Large Eddy Simulations

Here the predictions using Large Eddy Simulations are presented. A time step of $\Delta t = 0.0026H/U_{in}$ was used which gave a maximum convective CFL number of $CFL_{max} \simeq 0.9$. As initial flow field an instantaneous 2D laminar flow field was employed. The predicted results presented here have been averaged for a period of $T = 65H/U_{in}$, and also averaged in the spanwise direction between $0.15 \leq z/W \leq 0.85$; this is denoted as $\langle . \rangle_{zt}$.

The predicted vector field is presented in Fig. 2, and as can be seen, the wall jet stays attached to the ceiling up to $x/H \simeq 1.4$. In Fig. 2 the peak velocity in the wall jet is also shown. The peak velocity decays as $x^{-1/2}$ and the dashed line represents the curve $\langle \bar{u} \rangle_{zt}/U_{in,max} = K_p(x/h)^{-1/2}$ with $K_p = 2.03$. The corresponding experimental value is $K_p = 2.39$ (Topp, Nielsen, and Davidson 2000). Please note that at the inlet a parabolic profile is prescribed in the predictions, and $U_{in,max}$ denotes the maximum value of the inlet profile.

In Fig. 3 the predicted $\bar{u}$ profiles are compared with experiments (Topp, Nielsen, and Davidson 2000). The agreement is, as can be seen, fairly good, at least up to $x/H = 0.6$. Downstream of this position it seems that the experimental wall jet more or less vanishes, and the experimental velocities decays much faster for increasing x than the predicted ones.

In Fig. 4 the predicted time history of $\bar{u}$ at two different points in the room are presented. Point P1 is located in the wall jet, and and the flow seems to be fully turbulent. However, when looking at the energy spectrum for that point, it is clearly seen that the flow is not fully turbulent, as the spectrum does not show any $-5/3$ region, see Fig. 5. The probability of $\bar{u}$ at Point P1 (Fig. 4) exhibits the usual form, with a well-defined peak at the mean value of $\bar{u}_{mean}/U_{in} \simeq 0.3$ (which is also seen from the time history), and its distribution is close to Gaussian. Point P2 in Fig. 4 is located in the region where the wall jet separates. Here the frequency of $\bar{u}$ is much lower. From the time history it is seen that the velocity at some instances go down to large negative values ($\bar{u}/U_{in} \simeq -0.25$). This is also sen from the probability function, where a tail of large negative $\bar{u}$ can be seen. The probability is very low, almost zero; this is because, as can be seen from the time history, it happens only once.

The spectrum in Fig. 5 for point P2 shows a region where the spectrum exhibits a $-5/3$ behavior, which should indicate that the flow were fully turbulent. However, from the time
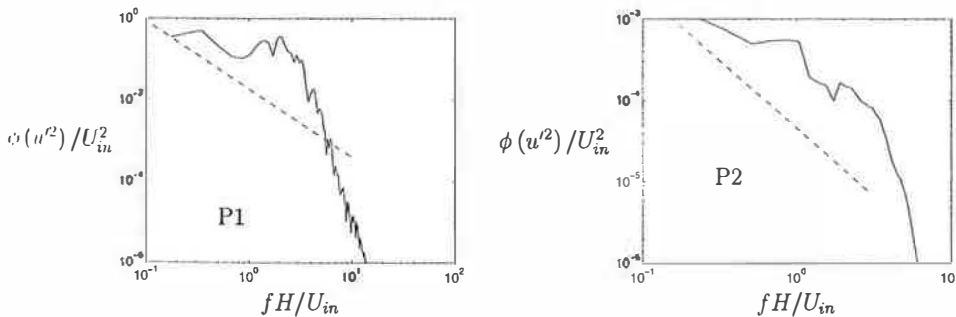

FIGURE 5: Density spectrum of $\bar{u}$ at two points P1 & P2 (see Fig. 4). The dashed lines show $\phi \propto f^{-5/3}$.
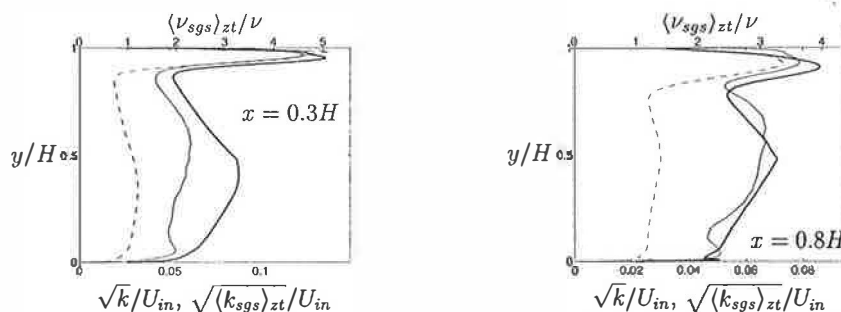
FIGURE 6: Turbulent profiles at $z = 0.5W$. Thick solid line: $(\nu_{sgs})_{zt}/\nu$; thin solid line: $\sqrt{k}/U_{in}$, dashed line: $\sqrt{\langle k_{sgs}\rangle_{zt}}/U_{in}$.

history in Fig. 4, it seems that the flow cannot be characterized as turbulent, because no high frequencies are present. The flow at this point, which is in the separation region, is dominated by large, unsteady structures. This can also be seen when the flow in the mid-plane ($z = W/2$), is visualized as a movie. The flow in the whole room can probably best be characterized as transitional.

In Fig. 6 profiles of the square root of the resolved turbulent, kinetic energy $k = (\langle u'^2\rangle_{zt} + \langle v'^2\rangle_{zt} + \langle w'^2\rangle_{zt})/2$ are shown. As mentioned above, the flow is not believed to be fully turbulent, but it should rather be called transitional. Thus, although we call it "turbulent kinetic energy", k should here be taken as a measure of the kinetic energy of the large, unsteady structures (the streamwise fluctuation, for example, is defined as $\langle u'^2\rangle_{zt} = \langle(\bar{u} - \langle\bar{u}\rangle_{zt})^2\rangle_{zt}$). From Fig. 6 it can be seen that the SGS kinetic energy k_{sgs} is rather large compared to k, and in the wall jet at $x = 0.3H$ k_{sgs} is even larger. However, the SGS stresses (not shown here) are much smaller that the corresponding resolved stresses. The SGS viscosity ν_{sgs} is also shown in Fig. 6, and as can been it is everywhere smaller than 5ν. This is typical in a well-resolved LES. Recall that in RANS, the turbulent viscosity is typically two to three orders of magnitude larger than the physical viscosity.

CONCLUSIONS

In the present work the flow in a ventilated room at low Reynolds number ($Re = 600$) has been simulated both with 2D unsteady laminar approach, RANS and LES. Only LES proved to be capable of predicting this flow.

Acknowledgment

REFERENCES
Davidson, L. (1997). Large eddy simulation: A dynamic one-equation subgrid model for three-dimensional recirculating flow. In *11th Int. Symp. Turb. Shear Flow*, Vol. 3, Grenoble, pp. 26.1–26.6.

Krajnović, S. and L. Davidson (1999). Large-eddy simulation of the flow around a surface-mounted cube using a dynamic one-equation subgrid model. In S. Banerjee and J. Eaton (Eds.), *The First International Symp. on Turbulence and Shear Flow Phenomena*, New York, pp. 741–746.

Peng, S.-H., L. Davidson, and S. Holmberg (1997). A modified Low-Reynolds-Number $k - \omega$ model for recirculating flows. *ASME: Journal of Fluids Engineering 119*, 867–875.

Sohankar, A., L. Davidson, and C. Norberg (2000). Large eddy simulation of flow past a square cylinder: Comparison of different subgrid scale models (to appear). *ASME: J. of Fluids Engng 122*(1).

Topp, C., P. Nielsen, and L. Davidson (2000). Room airflows with low Reynolds number effects (to appear). In *7th Int. Conf. on Air Distributions in Rooms, ROOMVENT 2000*, Reading, U.K.